1S 33

Critical β-scaling on toroidal magnetic field*

L. E. Zakharov,

R. Budny, E. Fredrickson

Princeton University,

Princeton Plasma Physics Laboratory

1996 APS meeting, Denver

*This work supported by DOE contract DE--AC02--76--CHO--3073.

Abstract

It was found on TFTR[2] that at the lower toroidal magnetic field, the discharges with presumably same pressure and current density profiles disrupt at higher β's than at the high toroidal field. The conventional MHD approach cannot explain this fact assuming similarity of the profiles. Earlier, we found that despite large plasma sizes and magnetic field, the stabilizing FLR effects are important in TFTR. Also, triggering the disruptions in TFTR supershots was explained by the coupling between the $m = 1$ mode and ballooning modes[3]. Thus, it was established that in high performance shots, the β-limit is determined essentially by the ballooning modes. We developed a two-fluid collisionless model for ballooning instabilities which was implemented into the Sweeping Equilibrium and Stability Code (SESC). These model does show an increase in β at lower magnetic field. In particular, for the same plasma profiles it predicts 30 % higher β at $B = 2\ T$ than at $B = 5\ T$, which is consistent with observations. This explanation can be verified experimentally by changing the relative contributions of the plasma density and the temperature into the total pressure.

[2]E. D. Fredrickson. MHD workshop on Beta Limits in Long Pulse Discharges, San Diero, 1995

[3]L. Zakharov, R. Budny, et all. 23rd EPS Conf. on Contr. Fusion and Pl. Physics, Kiev, 1996

1. OUTLINE

- Two Fluid ballooning equations.
- FLR modification of ideal modes.
- Disruptions triggering in TFTR
- $\beta_N(B)$ dependence for TFTR.

2. Two Fluid ballooning equations

Linearized Braginskii equations

$$
\begin{aligned}
& m_i n_i \gamma \tilde{\mathbf{V}} + \nabla \tilde{p} = \frac{1}{c}(\tilde{\mathbf{j}}_\perp \times \mathbf{B}) + \frac{1}{c}(\mathbf{j} \times \tilde{\mathbf{B}}) \\
& + \frac{4\pi n_e e \gamma d_e^2}{c^2} \tilde{\mathbf{j}}_\parallel, \\
& \frac{m_i \gamma}{Ze} \tilde{\mathbf{V}} + \nabla \tilde{\phi} + \frac{\gamma - i\omega_{*i}}{c} \tilde{\mathbf{A}} = \frac{1}{c}(\tilde{\mathbf{V}}_\perp \times \mathbf{B}) \\
& + \frac{p_i' \tilde{n}_e - n_e' \tilde{p}_i}{n_e^2 e} \nabla a - \frac{4\pi \nu_{ei} d_e^2}{c^2} \tilde{\mathbf{j}}_\parallel, \\
& (\gamma - i\omega_{*i}) \tilde{p}_i = -p_i' \tilde{V}^a - \Gamma_i p_i (\nabla \cdot \tilde{\mathbf{V}}), \\
& (\gamma - i\omega_{*e}) \tilde{p}_e = -p_e' \tilde{V}_{e\perp}^a - \Gamma_e p_e (\nabla \cdot \tilde{\mathbf{V}}_e), \\
& (\gamma - i\omega_{*e}) \tilde{n}_e = -n_e' \tilde{V}_{e\perp}^a - n_e (\nabla \cdot \tilde{\mathbf{V}}_e), \\
& (\gamma - i\omega_{*i}) \tilde{n}_e = -n_e' \tilde{V}_\perp^a - n_e (\nabla \cdot \tilde{\mathbf{V}}).
\end{aligned}
\tag{2.1}
$$

characteristic scale lengths

$$
\begin{aligned}
\rho_s^2 &\equiv \frac{c_s^2}{\Omega_{ci}^2}, \quad c_s^2 \equiv \frac{p}{m_i n_i}, \\
d_e^2 &\equiv \frac{c^2}{\omega_{pe}^2}, \quad \hat{d}^2 \equiv d_e^2 \left(1 + \frac{\nu_{ei}}{\gamma}\right).
\end{aligned}
\tag{2.2}
$$

Characteristic frequencies

$$
\begin{aligned}
i\omega_{*i} &\equiv -\frac{cp_i'}{n_e e\bar{\Psi}'}\frac{\partial}{\partial\phi}, \quad & i\omega_{*e} &= \frac{cp_e'}{n_e e\bar{\Psi}'}\frac{\partial}{\partial\phi} \\
i\omega_{*i}^n &\equiv -\frac{cT_i n_i'}{n_e e\bar{\Psi}'}\frac{\partial}{\partial\phi}, \quad & i\omega_{*e}^n &\equiv \frac{cT_e n_e'}{n_e e\bar{\Psi}'}\frac{\partial}{\partial\phi}
\end{aligned}
\tag{2.3}
$$

ν_{ei}.

FLR parameters

$$
m^2\frac{\rho_s^2}{r^2}, \quad \tau_A^2\omega_{*i}^2 \propto m^2, \quad \frac{\nu_{ei}}{2\omega_{*\ldots}} \propto \frac{1}{m}. \tag{2.4}
$$

In TFTR high-performance supershots

$$
\frac{\rho_s^2}{r^2}_{(1/3a)} \simeq \frac{m^2}{40^2}, \quad \frac{\nu_{ei}}{2\omega_{*\ldots}} \simeq 1 - -20. \tag{2.5}
$$

Plasma pressure perturbation

$$
\begin{aligned}
\tilde{n}_e &= -\frac{n_e'}{\gamma - i\omega_{*i}}\tilde{V}_\perp^a - \frac{n_e}{\gamma - i\omega_{*i}}(\nabla\cdot\tilde{\mathbf{V}}),\\
(\nabla\cdot\tilde{\mathbf{V}}_e) &= -\frac{incn_e'\tilde{p}}{n_e^2 e\sqrt{g}B^\theta} + \frac{n_e'(i\omega_{*i} - i\omega_{*e})}{n_e(\gamma - i\omega_{*i})}\tilde{V}_\perp^a\\
&\quad + \frac{\gamma - i\omega_{*e}}{\gamma - i\omega_{*i}}(\nabla\cdot\tilde{\mathbf{V}}),\\
\tilde{p}_i &= -\frac{p_i'}{\gamma - i\omega_{*i}}\tilde{V}_\perp^a - \frac{\Gamma_i p_i}{\gamma - i\omega_{*i}}(\nabla\cdot\tilde{\mathbf{V}}),\\
\tilde{p} &= -\frac{p'}{\gamma - i\omega_{*i}}\tilde{V}_\perp^a - \frac{m_i n_i c_s^2(\gamma - i\omega_{*e})}{(\gamma - i\omega_{*i})(\gamma - i\omega_{*e}^n)}(\nabla\cdot\tilde{\mathbf{V}}),\\
p_i'\tilde{n}_e - n_e'\tilde{p}_i &= \frac{p_i\Gamma_i n_e' - n_e p_i'}{\gamma - i\omega_{*i}}(\nabla\cdot\tilde{\mathbf{V}}).
\end{aligned}
\tag{2.6}
$$

Plasma velocity is determined by the Ohm law

$$\tilde{\mathbf{V}}_\perp \simeq c\frac{(\mathbf{B}\times\nabla\tilde{\phi})}{\mathbf{B}^2}, \quad \mathbf{B}\cdot(\nabla\times\tilde{\mathbf{V}}_\perp)\simeq c\nabla^2\tilde{\phi}. \tag{2.7}$$

Longitudinal equation of motion and Ohm's law

$$\begin{aligned} B^\phi\tilde{\psi} &= -(\mathbf{B}\cdot\nabla)\left(\frac{c\tilde{\phi}}{\gamma-i\omega_{*i}}+\frac{m_i c c_s^2}{Ze}\frac{\tilde{X}}{\gamma-i\omega_{*e}^n}\right) \\ &\quad + \lambda_e^2 B^\phi\nabla^2\tilde{\psi}, \\ \frac{\mathbf{B}\tilde{\mathbf{V}}}{\mathbf{B}^2} &= -\frac{(\mathbf{B}\cdot\nabla)\tilde{p}}{m_i n_i\gamma\mathbf{B}^2}-\frac{cnp'}{m_i n_i c\mathbf{B}^2\sqrt{g}\omega}\tilde{q}\tilde{\psi}, \\ \tilde{X} &\equiv \frac{(\nabla\cdot\tilde{\mathbf{V}})}{\gamma-i\omega_{*i}}, \quad \lambda_e^2\equiv\frac{\gamma+\nu_{ei}}{\gamma-i\omega_{*e}}d_e^2. \end{aligned} \tag{2.8}$$

Divergence of the plasma velocity

$$
\begin{aligned}
&\mathbf{g} \equiv \left(\mathbf{B} \times \nabla \frac{1}{\mathbf{B}^2}\right) - \frac{8\pi}{c}\frac{\mathbf{j}_\perp}{\mathbf{B}^2} = 2\frac{(\boldsymbol{\kappa} \times \mathbf{B})}{\mathbf{B}^2}, \\
&(\nabla \cdot \tilde{\mathbf{V}}_\perp) = -c\mathbf{g} \cdot \nabla\tilde{\phi} - \frac{m_i c\gamma}{Ze\mathbf{B}^2} c\nabla^2\tilde{\phi} \\
&- \frac{4\pi p}{\mathbf{B}^2}(\nabla \cdot \tilde{\mathbf{V}}) - (i\omega_{*i} - i\omega_{*i}^n)\tilde{X}, \\
&\tilde{X} = (\mathbf{B} \cdot \nabla)\frac{\mathbf{B}\tilde{\mathbf{V}}}{\mathbf{B}^2(\gamma - i\omega_{*i})} + \frac{(\nabla \cdot \tilde{\mathbf{V}}_\perp)}{\gamma - i\omega_{*i}}.
\end{aligned}
\tag{2.9}
$$

For divergence of the current density

$$\begin{aligned}
\tilde{\mathbf{j}} &= \mathbf{j}_\perp - \frac{B^\phi \nabla^2 \tilde{\psi}}{\mathbf{B}^2}\mathbf{B}, \\
\frac{1}{c}\mathbf{j}_\perp &= \frac{\mathbf{B}\times\nabla\tilde{p}}{\mathbf{B}^2} + m_i n_i \gamma \frac{\mathbf{B}\times\tilde{\mathbf{V}}}{\mathbf{B}^2} \\
&\quad - \frac{1}{c}\frac{\mathbf{B}\times(\mathbf{j}\times\tilde{\mathbf{B}})}{\mathbf{B}^2}, \\
-(\mathbf{B}\cdot\nabla)\frac{B^\phi\nabla^2\tilde{\psi}}{\mathbf{B}^2} &= 4\pi\mathbf{g}\cdot\nabla\tilde{p} + 4\pi m_i n_i\gamma\frac{c\nabla^2\tilde{\phi}}{\mathbf{B}^2} \\
&\quad - 4\pi m_i n_i \gamma \frac{c(p_i\Gamma_i n_e' - n_e p_i')}{n_e^2 e\mathbf{B}^2}(\nabla a\cdot\nabla\tilde{X}).
\end{aligned} \tag{2.10}$$

Two-fluid high-n MHD equations

$$c\tilde{\phi} \equiv -(\gamma - i\omega_{*i})\tilde{U},$$
$$\mathbf{g} \equiv \left(\mathbf{B} \times \nabla \frac{1}{\mathbf{B}^2}\right) - \frac{8\pi}{c}\frac{\mathbf{j}_\perp}{\mathbf{B}^2} = 2\frac{(\boldsymbol{\kappa} \times \mathbf{B})}{\mathbf{B}^2}. \quad (2.11)$$

Equation of motion

$$\frac{(\mathbf{B}\cdot\nabla)}{B^\theta}\frac{\sqrt{g}B^\theta B^\theta \mathbf{k}^2}{\mathbf{B}^2 n^2}\tilde{q}\tilde{\psi} = -4\pi\sqrt{g}\frac{\mathbf{g}\cdot\mathbf{k}}{n}\frac{\tilde{p}}{in} \quad (2.12)$$
$$+ 4\pi m_i n_i \omega(\omega_{*i} - \omega)\sqrt{g}\frac{\mathbf{k}^2\tilde{U}}{\mathbf{B}^2 n^2}.$$

Ohm's law

$$(1 + \lambda_e^2\mathbf{k}^2)\tilde{q}\tilde{\psi} =$$
$$\frac{(\mathbf{B}\cdot\nabla)}{B^\theta}\left(\tilde{U} - \frac{nm_i c c_s^2}{Ze(\omega - \omega_{*e}^n)}\frac{\tilde{X}}{in}\right). \quad (2.13)$$

Coupling with the sound waves

$$\frac{c_s^2}{\omega(\omega-\omega_{*e}^n)}\frac{(\mathbf{B}\cdot\nabla)}{B^\theta}\frac{\sqrt{g}B^\theta B^\theta}{\mathbf{B}^2}\frac{(\mathbf{B}\cdot\nabla)}{B^\theta}\frac{\tilde{X}}{in} + \frac{P_s\lambda_e^2}{4\pi m_i n_i\omega(\omega_{*i}-\omega)}\frac{(\mathbf{B}\cdot\nabla)}{B^\theta}\frac{\sqrt{g}B^\theta B^\theta\mathbf{k}^2\tilde{q}\tilde{\psi}}{\mathbf{B}^2} = - \sqrt{g}\left(\frac{\omega-\omega_{*i}^n}{\omega-\omega_{*i}}+\frac{4\pi p}{\mathbf{B}^2}\right)\frac{\tilde{X}}{in} + \sqrt{g}\frac{\mathbf{g}\cdot\mathbf{k}}{n}\tilde{U} - \frac{nm_i c\omega}{Ze}\frac{\sqrt{g}\mathbf{k}^2}{n^2\mathbf{B}^2}\tilde{U}. \tag{2.14}$$

Pressure perturbation

$$\frac{4\pi\tilde{p}}{in} = P_s\tilde{U} - \frac{\omega-\omega_{*e}}{\omega-\omega_{*e}^n}4\pi m_i n_i c_s^2\frac{\tilde{X}}{in}. \tag{2.15}$$

Equations (2.11)--(2.15) describe:

- ideal ballooning modes
- resistive and collisionless nonideal ballooning modes
- FLR modified ballooning modes
- FLR stabilization of ballooning modes

3. FLR modification of ideal modes

Ideal limit

$$\lambda_e = 0,$$

of these equations in the absence of ω_* effects

$$\begin{aligned}
&\frac{(\mathbf{B}\cdot\nabla)}{B^\theta}\frac{\sqrt{g}B^\theta B^\theta \mathbf{k}^2}{\mathbf{B}^2 n^2}\tilde{q}\tilde{\psi} = -4\pi\sqrt{g}\frac{\mathbf{g}\cdot\mathbf{k}}{n}P_s\tilde{U},\\
&\tilde{q}\tilde{\psi} = \frac{(\mathbf{B}\cdot\nabla)}{B^\theta}\left(1+\rho_s^2\mathbf{k}^2\right)\tilde{U},\\
&P_S \equiv \frac{8\pi^2 dp}{d\Psi},\\
&\rho_s^2 = \frac{c_s^2}{\Omega_{ci}^2}
\end{aligned} \tag{3.1}$$

gives FLR modified ideal ballooning modes.

ω_* - stabilization of ideal modes is seen from a simplified version of ballooning equation

$$[f(r,\theta)\xi']' = p'g(r,\theta)\xi + n^2\tau_A^2\frac{\omega_{*i}^2}{4}\xi \qquad (3.2)$$

and explains wave numbers ($n < 10$) of the "KBM" modes being observed in TFTR.

At $B_{tor} > 5T$, the ballooning modes in TFTR are barely affected by FLR effects inside 30 cm zone.

At lower B_{tor}, FLR stabilization is more effective

$$\frac{\rho_s^2}{r^2} \propto \frac{T}{B_{tor}^2} \propto \frac{1}{B_{tor}}, \quad \tau_A^2\omega_{*i}^2 \propto \frac{n_i T_i'^2}{B_{tor}^4} \propto \frac{1}{B_{tor}}$$

and can lift ballooning mode limits in favor of the REAL low-n limits.

4. Disruptions triggering in TFTR

Characteristic features of TFTR supershots:

- highly peaked pressure profile
- $q_0 \simeq 0.8 - 0.9$ with $r_{1/1} \simeq 0.15a - 0.30a$

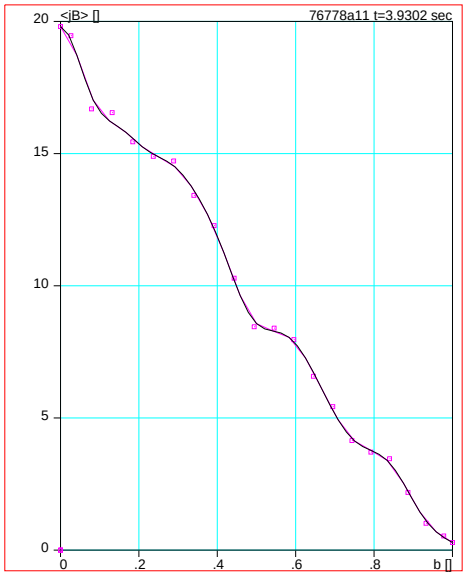

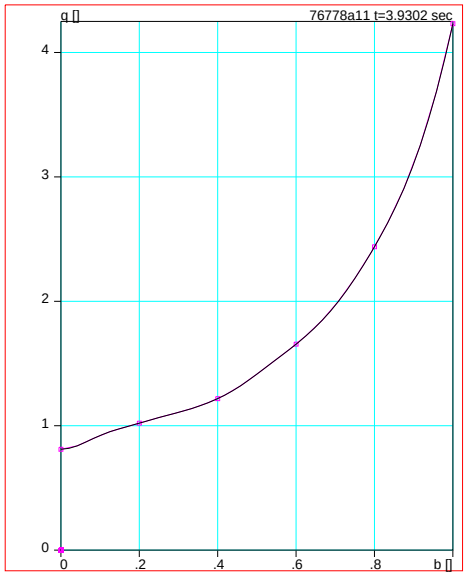

$< jB >$-profile q(r)-profile

Because of the high peakedness of the pressure profile, TFTR is limitted by the ballooning limit, not by the low-n limit.

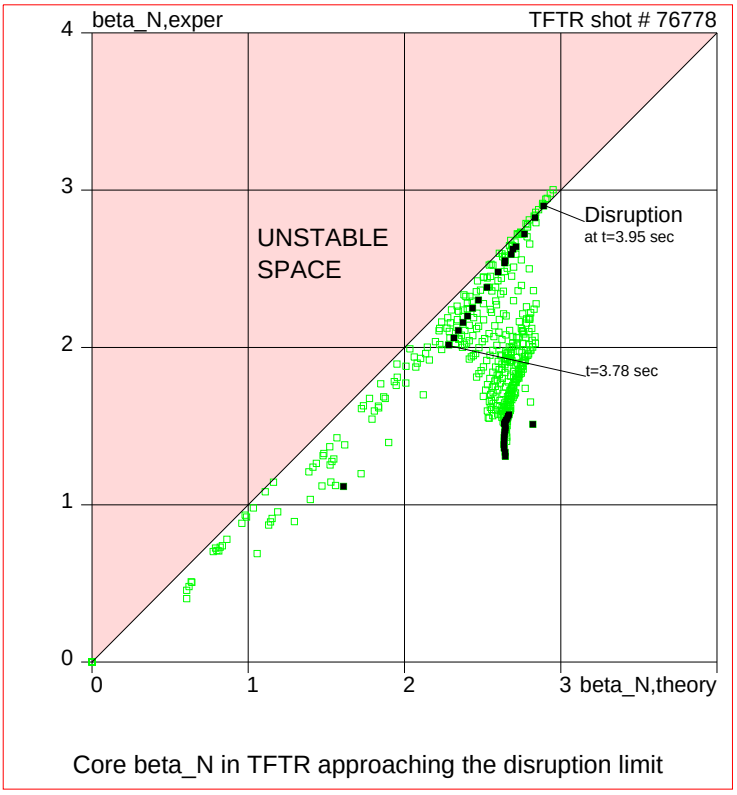

Core beta_N in TFTR approaching the disruption limit

Phase space β_N---$\beta_{N,critical}$ and a trajectory of $\beta_N(1/3)$ (Black points) approaching the stability boundary for 9.2 MW of the fusion power TFTR supershot #76778, which was terminated by a major disruption.

Two-fluid MHD predicts

- mode localization
- the mode frequency and
- the upper level of the n wave number.

of so-called "KBM" ballooning modes in TFTR

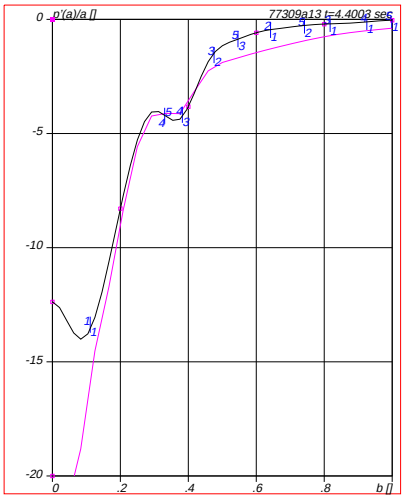

77309a13 n=5 Ballooning

$n = 5$

Unstable

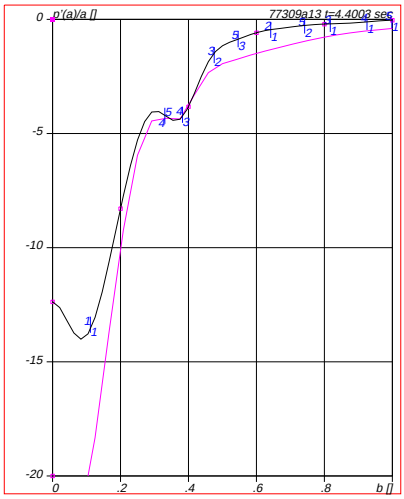

77309a13 n=8 Ballooning

$n = 8$

Unstable

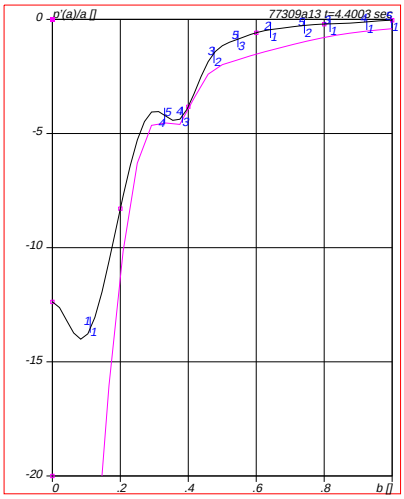

77309a13 n=10 Ballooning

$n = 10$

Stable

5. $\beta_N(B)$ dependence for TFTR

At high magnetic field, TFTR supershot regimes are essentailly limitted by the ballooning modes near the plasma center.

Given TFTR peaked pressure profiles, ballooning stability depends on magnetic field due to ω_* effects

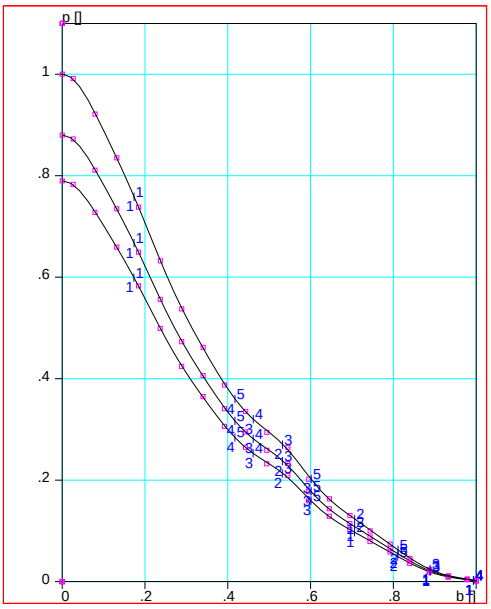

TFTR marginally stable pressure profiles for $B_{tor} = 5, 3.3, 2.2\,T$

Critical $\beta_N(B)$ depends on both toroidal magnetic field and the plasma density

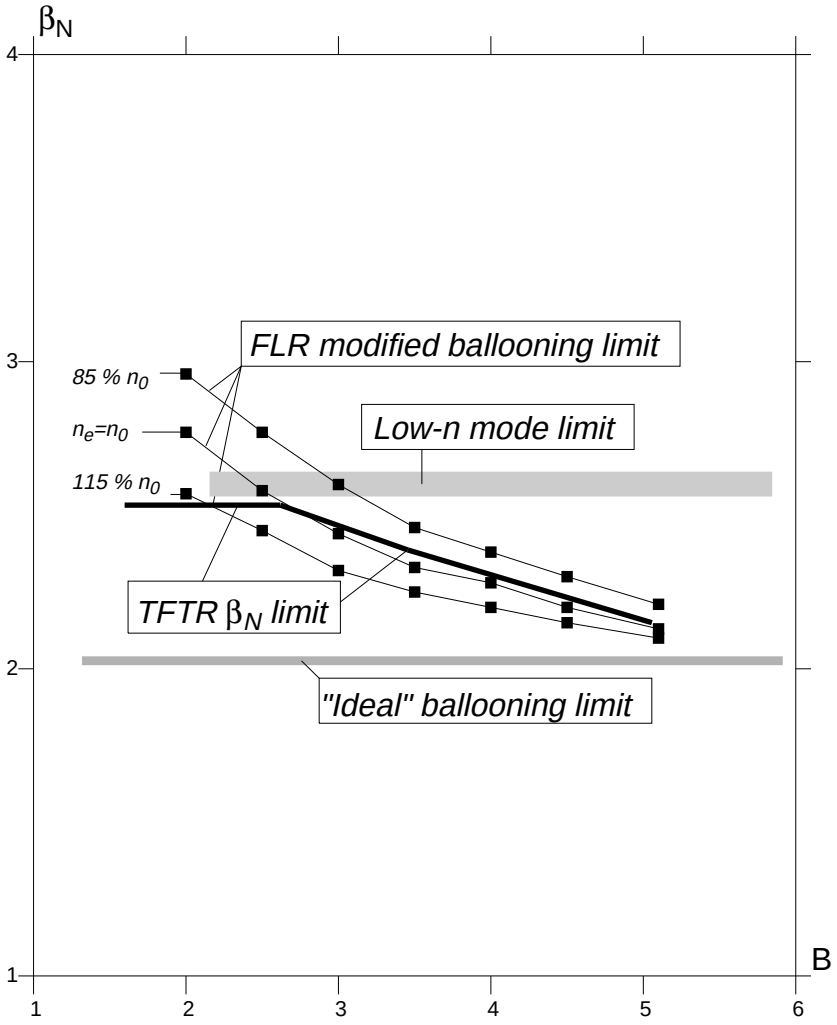

TFTR β_N (B_{tor}) dependence

6. Summary

Two-fluid MHD model gives a self-consistent picture of MHD activity in TFTR

- Earlier, it explained sawtooth stabilization, observable mode frequency and wave numbers of (KBM) ballooning modes, triggering high-β disruption
- it is consistent with the critical $\beta_N(B_{tor})$ dependence in TFTR.
- At low-B_{tor} it predicts more stability for higher temperature at the same β.

At low-B_{tor}, the this model can be verified in experiment by exploring β_N dependence on the plasma temperature (or density).